

## CLOSURE INVARIANTS FOR POLARISED RADIO INTERFEROMETRIC OBSERVATIONS: A GRAPH THEORETICAL APPROACH

VINAY KUMAR<sup>1\*</sup>, RAJARAM NITYANANDA<sup>1†</sup>, AND JOSEPH SAMUEL<sup>1,2‡</sup>

<sup>1</sup>International Centre for Theoretical Sciences, Tata Institute of Fundamental Research, Bengaluru 560089, India and

<sup>2</sup>Raman Research Institute, Bengaluru 560080, India

*Version July 2, 2024*

### Abstract

Aperture synthesis observations with full polarisation have long been used to study the magnetic fields of synchrotron emitting sources. Recently proposed closure invariants give us a powerful method for extracting information from measured visibilities which are corrupted by antenna and polarisation dependent gains. In this paper, a formalism developed earlier for complete graphs (where all visibilities are available) is extended to incomplete graphs. The formalism provides a complete and independent set of closure invariants from the measured visibilities in a general situation where not all visibilities are available. We then show in a simulated, quasi-realistic case that the invariants developed here contain usable information even in the presence of noise.

*Subject headings:* Aperture Synthesis, Polarisation, Closure Invariants

### 1. INTRODUCTION

Full polarisation observations with the Event Horizon Telescope have revealed the magnetic field structure of the innermost accretion flow around the M87 black hole (The Event Horizon Telescope Collaboration (2021)). The principle underlying such observations is described in the standard text (Thompson *et al.* (2017)) and is summarised below. The measured electric fields  $\mathbf{E}_a$  at a given antenna ‘ $a$ ’ are  $2 \times 1$  complex matrices which are related to the true fields  $\mathbf{T}_a$  by  $2 \times 2$  complex ‘gain’ matrices  $\mathbf{G}_a$ , i.e  $\mathbf{E}_a = \mathbf{G}_a \mathbf{T}_a$ . The measured correlations  $\mathbf{M}_{ab} = \langle \mathbf{E}_a \mathbf{E}_b^\dagger \rangle$  are thus modified versions of the true correlations  $\mathbf{S}_{ab} = \langle \mathbf{T}_a \mathbf{T}_b^\dagger \rangle$  given by the matrix product  $\mathbf{M}_{ab} = \mathbf{G}_a \mathbf{S}_{ab} \mathbf{G}_b^\dagger$ . Here  $\langle f \rangle$  is our notation for the average of  $f$  over the observation time.

An important role is played in the imaging process by ‘closure quantities’. These are constructed from products of measured correlations around closed loops of antennas designed to cancel all the gains, rendering them invariant with respect to any changes in gains. These have long been known for the single polarisation case (Thompson *et al.* (2017)), but were only recently introduced for full polarisation by Broderick and Pesce (2020), and in full generality by Thyagarajan *et al.* (2022) and Samuel *et al.* (2022) for the case when all correlations are measured. We regard the antenna array as a graph, with antennas as vertices, and measured baselines as edges. The existing formalism is for the ‘complete graph’ where every pair of vertices is joined by an edge. In this work, we extend the framework by constructing a complete and independent set of closure invariants in the more general case of an incomplete graph, i.e when not all correlations

between pairs are available. In a heterogeneous array, this could happen for correlations between the smallest antennas. We also explore the noise properties of the invariants, which are nonlinear functions of the correlations. This step is necessary to construct likelihood functions for models to compare to measurements.

The principle of gain cancellation is that along any circuit, we construct a matrix product around a closed loop. A measured correlation matrix  $\mathbf{M}_{ab}$  is followed with the inverse adjoint of  $\mathbf{M}_{bc}$ , i.e the matrix  $(\mathbf{M}_{bc}^\dagger)^{-1}$  which we denote, for brevity, by  $\widehat{\mathbf{M}}_{bc}$ . This ensures that the terminal  $\mathbf{G}_b^\dagger$  of  $\mathbf{M}_{ab}$  is cancelled by the initial  $\mathbf{G}_b^{\dagger -1}$  of  $\widehat{\mathbf{M}}_{bc}$ . Coming back to the starting point ‘ $a$ ’ after an even number of baselines, we now only have an initial  $\mathbf{G}_a$  and a final  $\mathbf{G}_a^{-1}$ . We call such a product around an even number of baselines a ‘covariant’. To construct invariants, we can take the trace and the determinant of this product, both of which are independent of  $\mathbf{G}_a$  (Broderick and Pesce (2020)). The novel contribution of Samuel *et al.* (2022) which was used to find the complete, independent set of invariants was to introduce products of measured correlation matrices over loops with an *odd* number of baselines (e.g triangles), named as ‘advvariants’. These start with a  $\mathbf{G}_a$  and end with a  $\mathbf{G}_a^\dagger$ . Invariants were constructed from these advvariants using properties of Lorentz transformations, as explained below.

### 2. THE INCOMPLETE GRAPH CASE

The left side of Figure 2 shows the case of five antennas as vertices of a connected graph. (A disconnected graph would require each connected piece to be treated separately). Since this has all 15 baselines as the edges, it is a complete graph. For the general complete graph with  $N$  antennas, we can choose a base point and draw edges to each of the  $(N - 1)$  remaining antennas. That is shown

\* vinay.kumar@icts.res.in  
 † rajaram.nityananda@icts.res.in  
 ‡ sam@icts.res.in

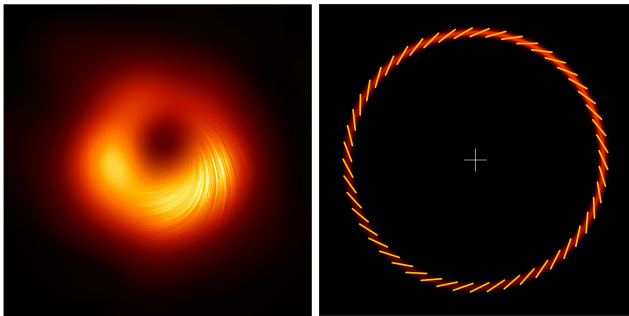


FIG. 1.— The image on the left shows the first polarised image of M87\* accretion flow taken by the EHT collaboration, adapted from under a CC-BY 4.0 license. On the right is the schematic diagram of the ring image used in our numerical work to emulate features of the figure on the left.

in solid lines and forms a spanning tree – a connected set of  $(N - 1)$  edges which visit all the  $N$  vertices. We thereby get  $(N - 1)(N - 2)/2$  remaining edges, shown dotted, each of which gives us one triangular circuit with respect to the base point. These are the advariants from which the complete set of invariants was constructed in Samuel *et al.* (2022).

To extend these ideas to the case of a connected incomplete graph, we proceed as follows. Given a graph  $\mathcal{G}$ , we pick a spanning tree – a connected subgraph  $\mathcal{G}_0 \subset \mathcal{G}$  which contains all the vertices but has no closed loops. With  $N$  antennas, this has  $(N - 1)$  edges. The spanning tree, by itself cannot give us any invariants, as it has no closed loops. For the same reason, there is a unique path in the spanning tree to travel from one vertex to any other.

The remaining edges, not in the spanning tree, are shown as dotted lines in the figure. We now put back these edges, each of which gives us a closed loop. This is obtained by travelling from the base point along the unique path to one of the vertices of this edge, traversing the edge, and then returning to the base point, again by a unique path. The final closed path from the base back to the base may have an odd or an even number of edges. Each loop with an even number of edges give us a covariant and each loop with an odd number give us an advariant.

If there are no advariants, all the loops in  $\mathcal{G}$  have an even length. In this special case, one can consistently colour all the vertices of  $\mathcal{G}$  alternately red and blue so that edges only connect vertices of different colours. This is the definition of a bipartite graph. In this case one only has covariants. Invariants are produced by taking the trace and determinant of these covariants. If the graph is not bipartite, there is at least one odd loop in  $\mathcal{G}$ . One can convert all the covariants into advariants by concatenation – first traversing the odd loop and then traversing any even loop. Invariants are then constructed by the earlier method based on Lorentz transformations and four-vectors Samuel *et al.* (2022). To summarise, we only need to deal with two cases: one with only covariants (bipartite graph), and one with only advariants (non-bipartite graph).

The right side of Figure 2 gives an example of an incomplete graph with five antennas and only six baselines measured. A spanning tree – not unique – for the graph is shown using solid lines. The remaining edges are shown dotted. From a given base point – again not unique –

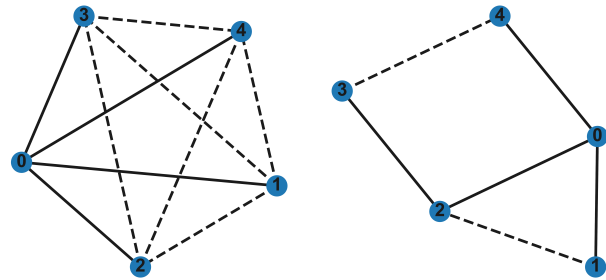


FIG. 2.— Figure shows an array of five telescopes represented as vertices. The lines joining the vertices represent measured baselines. The graph on the left is a complete graph with all ten baselines measured. The graph on the right shows only six baselines measured. In both graphs, the solid lines form a spanning tree: a subgraph that contains all the vertices, but no closed loops. The graph on the left gives us six advariants, while the graph on the right gives us one advariant and one covariant.

one can make one circuit for each of the dotted edges. The matrix products around each of these loops are independent, since each contains one baseline not present in any other loop. These loops also form a kind of basis – any other closed loop can be built up by traversing these basic loops successively. (More formally, these loops are *generators* of the fundamental group of the graph )

### 3. CONSTRUCTION OF INVARIANTS

Picking a common starting point for a complete set of circuits, we now have cancellation of the intermediate  $\mathbf{G}$ 's for all the circuits. We are still left with factors of either a  $\mathbf{G}$  and a  $\mathbf{G}^\dagger$ , or, a  $\mathbf{G}$  and a  $\mathbf{G}^{-1}$  at the two ends of a matrix product with alternating correlation matrices and their hatted forms. It now remains to construct scalar quantities from such a product which are independent of the terminal  $\mathbf{G}$ 's. For advariants, the procedure to construct invariants is given in Samuel *et al.* (2022). This relies on the connection between  $2 \times 2$  matrices with determinant 1, and Lorentz transformations, long used in relativistic quantum theory. This connection was first introduced in radio astronomy in the context of single dish polarimetry by Britton (2000).

It is convenient, with no loss of generality, to expand the matrix product around a closed loop in terms of the identity and the three Pauli matrices, with four complex coefficients  $a_0, a_1, a_2, a_3$ . Premultiplying by  $\mathbf{G}$  and postmultiplying by  $\mathbf{G}^\dagger$  then produces a real Lorentz transformation among the four  $a$ 's and further scales them by a positive constant  $\det(\mathbf{G}\mathbf{G}^\dagger)$ . If there are only advariants, as in the complete graph case (Samuel *et al.* (2022)), we construct a set of independent scalar products of these four vectors. Normalising (or taking ratios) to remove the overall scale is sufficient to give the desired number of invariants. The same procedure works for the incomplete graph case, if we have only advariants. As shown in Samuel *et al.* (2022), with  $N_A$  advariants, we get  $8N_A - 7$  real invariants. If there is even a single advariant, one can traverse it and then any covariant, and the resulting product is an advariant. By converting all covariants to advariants the earlier algorithm can be used.

The only case left is when there are only covariants, say  $N_C$  of them. This is unlikely to occur in practice,

but we present it below for completeness. All covariants transform with a prefactor of  $\mathbf{G}$  and a postfactor of  $\mathbf{G}^{-1}$ . A graph in which there are only covariants is necessarily a bipartite graph, as all closed loops have an even number of edges. In this case,  $a_0$  remains invariant, since it is half the trace. The determinant is also invariant, and it is  $a_0^2 - a_1^2 - a_2^2 - a_3^2$ . Therefore, the sum of the squares (not absolute squares!) of  $a_1, a_2, a_3$  is separately an invariant, so we refer to it as a (complex) three-vector. For a single covariant, this approach is equivalent to the determinant and trace, either way gives 4 real invariants. The traces by themselves contribute  $2N_C$  real invariants, Setting these aside, with more than one covariant, we can form the complex three dimensional scalar product from the three -vectors of two covariants, which is also an invariant. The first two covariants give us two complex vectors, which give us three complex invariants, their squared lengths and inner product. The two three-vectors are also enough to define a frame in this vector space, since we can take the third vector as their cross product. At this stage, with two covariants, we have six real invariants. Each of the remaining  $N_C - 2$  covariants now contributes six more real invariants, since one can construct scalar products with the three members of the frame. So, for  $N_C \geq 2$ , we have  $2N_C + 6 + 6(N_C - 2) = 8N_C - 6$  real invariants in all, As in the case of advariants,  $N_C = 1$  is an exceptional case, with 4 rather than 2 invariants.

#### 4. THE ROLE OF INVARIANTS IN IMAGING

The Event Horizon Telescope Collaboration (2021) have used different strategies to produce the iconic image shown below. The traditional route to determining and refining the antenna based gains is self calibration (Thompson *et al.* (2017)), in which, briefly, a model image and the gains are alternately updated. The gains are improved by fitting the model predictions to the measurements, while the image based on the current gains is improved by deconvolution. This strategy bypasses invariants – if the process converges, then all invariants are automatically satisfied by the final image.

However, invariants are still in use and have independent value especially in cases when the data is not extensive, the results may depend significantly on the details of the initial guess and the deconvolution algorithm. Accordingly, as recognised in the EHT work, there is a role for ‘forward modeling’ in which one computes the correlations from a parameterised family of models. (For a recent simulation of forward modeling using machine learning for parameter inference, see Thyagarajan *et al.* (2023)). For example, in a case like M87, the shape of the ring, the depth of the dark region inside it could be parameters. One can then compare the predicted invariants with those computed from the measured correlations. We have explored the use of invariants in this approach. Two questions need to be answered. a) given the presence of inverse matrices in the covariants and advariants, could near singular behaviour be an obstacle? b) Given that the invariants do not have an intuitive geometric meaning even in the single polarisation case, what features of the model can be reliably determined from them in a forward modeling framework?

#### 5. SIMULATIONS WITH NOISE

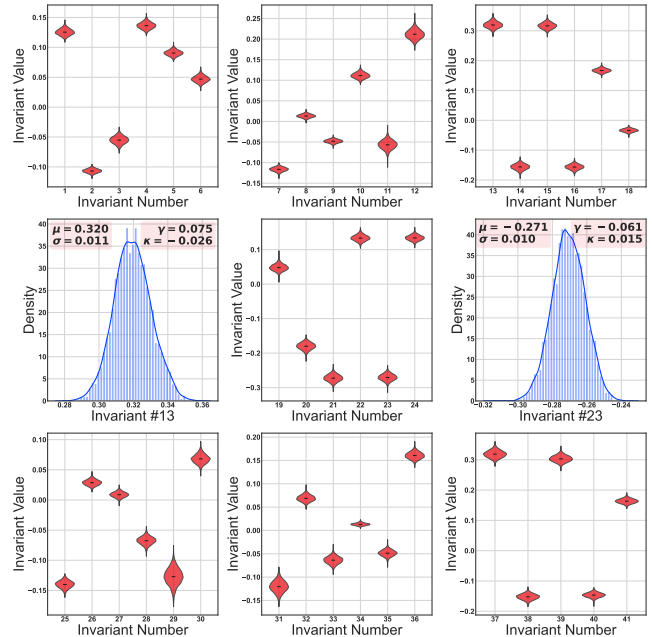


FIG. 3.— Violin plots showing the distribution of the 41 invariants for the complete graph case. The two bar plots show the distribution of two of the invariants in detail. The mean, standard deviation, skewness and kurtosis of these distributions are listed in the top right corners of the respective plots. The non-zero values of the skewness and the kurtosis indicate the non-gaussianities of the distribution.

A set of simulations was carried out on a toy version of the EHT  $u-v$  coverage. The polarised emission from the source was modelled as a ring with the thickness arising out of a gaussian intensity profile. The intensity also has a sinusoidal variation along the azimuth of the ring. This intensity distribution is shown in red in Figure 1. The yellow lines in the figure indicate the direction of polarisation. The free parameters related to the polarisation are the degree of linear polarisation (constant everywhere over the ring) and the azimuthal variation of the polarisation direction. The degree of circular polarisation is taken to be zero.

A snapshot based on  $u-v$  values for five locations - Hawaii, Chile, Mexico, two in the US mainland, and Spain - was used. The signal to noise was taken to be 100 for the strongest correlation and the same noise amplitude used for the weaker ones. Invariants were computed using the prescription in Samuel *et al.* (2022). The publicly available python package, NetworkX (Hagberg *et al.* (2008)), was used to construct the graphs, find spanning trees and compute invariants. A violin plot of the invariants is shown below, based on 5000 realisations of noise on the correlations.

The violin plots in Figure 3 gives a feel for the noise level. While the signal to noise on some of the invariants is poor, it is clear that there is no major issue with the inverse matrices which occur in the construction of the invariants. This can be rationalised from the fact that complex  $2 \times 2$  matrices form an 8 dimensional space, while the singular ones form a six dimensional space (from the vanishing of a complex determinant).

A similar exercise with an incomplete graph was carried out. This graph had 6 antennas in total, placed at randomly chosen points on the  $u-v$  plane. Out of the 15

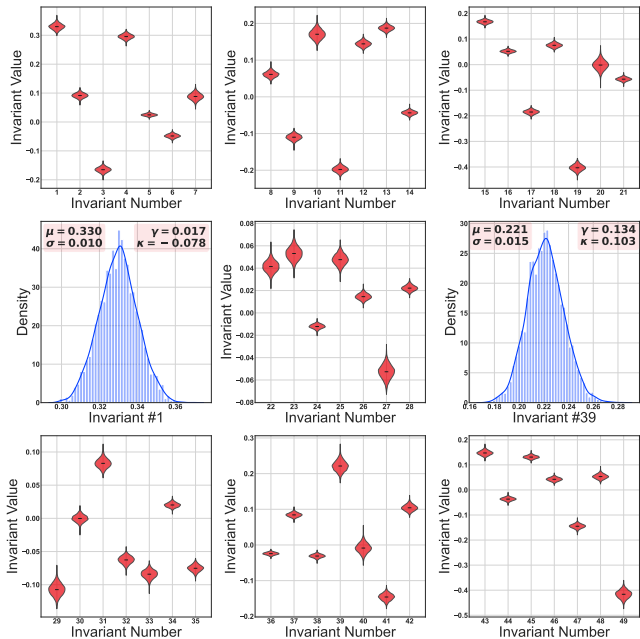


FIG. 4.— Violin plots showing the distribution of the 49 invariants for the incomplete graph case. As before, the two bar plots show the distribution of two of the invariants in detail, along with the mean, standard deviation, skewness and kurtosis.

- The Event Horizon Telescope Collaboration, *The Astrophysical Journal Letters* **910**, L12 (2021).
- A. R. Thompson, J. M. Moran, and J. Swenson, George W., *Interferometry and Synthesis in Radio Astronomy, 3rd Edition* (Springer Cham, 2017).
- A. E. Broderick and D. W. Pesce, *The Astrophysical Journal* **904**, 126 (2020).
- N. Thyagarajan, R. Nityananda, and J. Samuel, *Phys. Rev. D* **105**, 043019 (2022).

This paper was built using the Open Journal of Astrophysics L<sup>A</sup>T<sub>E</sub>X template. The OJA is a journal which

possible correlations, 12 were considered available. Noise properties were assumed to be the same as in the complete graph case. The invariants and their distributions are shown in Figure 4.

This already shows in a quasi realistic case, that the invariants constructed from advariants following the recipe in Samuel *et al.* (2022) do not have a major problem in the presence of noise. However, in forward modeling, an important role is played by the likelihood as a function of the parameters (see appendix to Thyagarajan *et al.* (2022), which argues for independence of the precise choice of invariants). For each set of parameter values, the likelihood has to be computed anew. Our simulations clearly show that some of the invariants have non gaussian distributions, and are clearly correlated, as shown by the computed covariance matrix. Computing a more realistic likelihood function is therefore a challenge which we are exploring.

## 6. ACKNOWLEDGEMENTS

We acknowledge support of the Department of Atomic Energy, Government of India, under project no. RTI4001. J. S. and R. N. acknowledge support by a grant from the Simons Foundation (677895, R.G.). We thank Nithyanandan Thyagarajan for sharing his work with us before publication, and for a lively discussion.

## REFERENCES

- J. Samuel, R. Nityananda, and N. Thyagarajan, *Phys. Rev. Lett.* **128**, 091101 (2022).
- M. C. Britton, *The Astrophysical Journal* **532**, 1240 (2000).
- N. Thyagarajan, L. Hoefs, and O. I. Wong, *Interferometric image reconstruction using closure invariants and machine learning* (2023), [arXiv:2311.06349](https://arxiv.org/abs/2311.06349) [astro-ph.IM].
- A. Hagberg, P. Swart, and D. S. Chult, *Exploring network structure, dynamics, and function using NetworkX*, Tech. Rep. (Los Alamos National Lab.(LANL), Los Alamos, NM (United States), 2008)

provides fast and easy peer review for new papers in the **astro-ph** section of the arXiv, making the reviewing process simpler for authors and referees alike. Learn more at <http://astro.theoj.org>.